Materials Science and Engineering C 46 (2015) 504–513

Contents lists available at ScienceDirect

Materials Science and Engineering C

journal homepage: www.elsevier.com/locate/msec

Dispersion fraction enhances cellular growth of carbon nanotube and aluminum oxide reinforced ultrahigh molecular weight polyethylene biocomposites

Anup Kumar Patel, Kantesh Balani *

Biomaterials Processing and Characterization Laboratory, Department of Materials Science and Engineering, Indian Institute of Technology Kanpur, 208016, India

ARTICLE INFO

Article history:
Received 23 July 2014
Received in revised form 4 October 2014
Accepted 28 October 2014
Available online 29 October 2014

Keywords:
Ultra high molecular weight polyethylene
Al_2O_3
MWCNTs
Wettability
Surface free energy
Cytocompatibility

ABSTRACT

Ultrahigh molecular weight polyethylene (UHMWPE) is widely used as bone-replacement material for articulating surfaces due to its excellent wear resistance and low coefficient of friction. But, the wear debris, generated during abrasion between mating surfaces, leads to aseptic loosening of implants. Thus, various reinforcing agents are generally utilized, which may alter the surface and biological properties of UHMWPE. In the current work, the cellular response of compression molded UHMWPE upon reinforcement of bioactive multiwalled carbon nanotubes (MWCNTs) and bioinert aluminum oxide (Al_2O_3) is investigated. The phase retention and stability were observed using X-ray diffraction, Raman spectroscopy and Fourier transform infrared (FTIR) spectroscopy. The reinforcement of MWCNTs and Al_2O_3 has shown to alter the wettability (from contact angle of ~88° ± 2° to ~118° ± 4°) and surface energy (from ~23.20 to ~17.75 mN/m) of composites with respect to UHMWPE, without eliciting any adverse effect on cytocompatibility for the L929 mouse fibroblast cell line. Interestingly, the cellular growth of the L929 mouse fibroblast cell line is observed to be dominated by the dispersion fraction of surface free energy (SFE). After 48 h of incubation period, a decrease in metabolic activity of MWCNT–Al_2O_3 reinforced composites is attributed to apatite formation that reduces the dispersion fraction of surface energy. The mineralized apatite during incubation was confirmed and quantified by energy dispersive spectroscopy and X-ray diffraction respectively. Thus, the dispersion fraction of surface free energy can be engineered to play an important role in achieving enhanced metabolic activity of the MWCNT–Al_2O_3 reinforced UHMWPE biopolymer composites.

1. Introduction

Biomaterials are used to direct, replace or supplement the function of living tissues of the human body. These are bone plates, sutures, heart valves, vascular grafts, joint replacements, intraocular lenses, ligaments, dental implants etc. [1,2]. These may be metals (Ti–6Al–4V, steel), ceramics (HAP, Al_2O_3), polymers (PMMA, polyolefins, nylon) as well as composites. UHMWPE, an engineering polymer, has unique combination of properties such as: highest slurry-abrasion resistance, exceptional impact resistance, low coefficient of friction, self-lubricating properties, outstanding stress-crack resistance, high resistance to cyclic fatigue failures and clearance for use in food and biomedical application [3]. The first hip prosthesis was implanted by using UHMWPE in the 1960s as an alternate to PTFE (polytetrafluoroethylene) and was found to be the best choice for total joint applications only for short term periods (~15–20 years) due to serious problem of wear debris formation and aseptic loosening, which leads to osteolysis [4]. Since the late 2000s profound research work was carried out to develop materials with enhanced tribological performance by crosslinking via gamma-irradiation, sterilizing with ethylene oxide, using cold atmospheric pressure, and gas plasma and organosilane treatment with partial damage of the outer surface of UHMWPE for in vitro as well as in vivo applications [5–7]. To maintain the original properties of materials, some alternative non-destructive routes were also developed to improve the wear performance of the composites. The reinforcement of a polymer matrix with inorganic (Al_2O_3, zirconia) as well as organic (carbon fibers and carbon nanotubes) fillers is the best route to fabricate prosthesis with super performance than virgin polyethylene components in total joint replacements [8,9].

The reinforcement of UHMWPE with 1 wt.% multiwalled carbon nanotubes (MWCNTs) drastically enhanced ductility (~140%) and modulus (~25%) [10]. It is well reported in literature that MWCNTs are extremely strong with tensile strength of ~200 GPa and Young's modulus of ~1 TPa and flexible (with break strain of ~10–30%) [11,12]. The effective utilization of MWCNTs into a matrix strongly depends on its homogeneous dispersion in the matrix, without destroying the integrity of matrices and MWCNTs–matrix interface bonding, which plays a major role in load transfer across MWCNTs–matrices interfaces during

* Corresponding author.
E-mail address: kbalani@iitk.ac.in (K. Balani).

http://dx.doi.org/10.1016/j.msec.2014.10.075
0928-4931/

application of mechanical stress [13–20]. Toughening of material is also improved by grafting with coupling agents like maleic anhydride (PE-g-MAH) and silanes and reinforcing with nano/micro-particles (3% SiC) as well as organic sheets by 0.2–9.0 wt.%, processed via compression molding [17,21–25]. Huang et al. reported that with 3% SiC with different coupling agents, an increase in the flexural strength by ~17% (16.7 to 19.6 MPa) than without a coupling agent was observed. Gupta et al. and Bakshi et al. [26–28], have reported the hybrid composites based on the UHMWPE–HAP–Al_2O_3–MWCNT system and found that an addition of 5 wt.% alumina has led to an increase in the hardness and modulus by 12% and 5.2%, respectively, while, 5 wt.% HAP addition has led to a decrease in the hardness and modulus by 44.5% and 53.8%, respectively, when compared to that of UHMWPE.

Ji-Hoon Lee et al. [29] have reported that reinforcement of silane modified MWCNTs in UHMWPE nanocomposites has resulted in significant lowering of specific wear rate by ~59%, when compared to that of virgin UHMWPE. It was observed that wear debris causes the immature failure of implants since the host cells produce cytokines (precursor of osteoclasts) that start consuming the bone around the implant and result in implant loosening [30,31]. Thus, in order to reduce the formation of wear debris, MWCNTs are reinforced into the UHMWPE matrix due to its lubricating property. It is reported that UHMWPE formed shish–kebab crystalline structure with MWCNTs [32], which enhances the mechanical properties of composites especially tensile modulus and fracture toughness. Enhanced crystallinity is observed after adding MWCNTs into the UHMWPE matrix [33–35]; on the other hand it is shown that the crystallinity of UHMWPE is not affected by the addition of MWCNTs [36].

Hydroxyapatite (HA) is one of the most important bioceramics for medical applications due to the similar chemical composition (Ca/P ratio of 1.67) to the mineral component of the natural human bone [37,38]. Extensive work has been reported on biomedical applications of HA and its composites via filler reinforcements, FGM formation, surface modification, grafting and coating [37–40]. The formation of apatite during incubation (cell culture) is checked by the SBF immersion test that predicts the activity of biomaterials in vitro [41]. Zadpoor and Szubert et al. [41,42] reported the apatite formation test at mica surface supported by physiological mineralization. It was observed that the layers of lipids such as dipalmitoylphosphatidylcholine (DPPC) on the inorganic material surfaces enhance the mineralization and crystal growth at 37 °C [41,42], but systematic quantitative analysis is not reported yet.

Above all, the surface free energy (SFE) of any biomaterial plays an important role in cell adhesion and proliferation, but a systematic analysis which correlates the polar and dispersion fractions of SFE with the density of metabolically active cells and apatite mineralization is not quantified. In the present work, multiwalled carbon nanotubes (MWCNTs) and Al_2O_3 were synergistically reinforced into a UHMWPE matrix in varying percentages via a compression molding process. The phases, chemical, and microstructure of the nanocomposites were characterized by X-ray diffraction analysis, FT-IR, Raman spectroscopy, and scanning electron microscopy. The biocompatibility and cellular response of composites were studied via L929 mouse osteoblast cell line (American Type Cell Collection—ATCC) in vitro cell culture experiments. The cell density was correlated with the surface free energy (SFE) of composites, which indicate that the cell adhesion mechanism in Al_2O_3–MWCNT–UHMWPE biopolymeric composites is strongly enhanced with increasing dispersion fraction of SFE.

2. Experimental section

2.1. Materials and processing

The UHMWPE medical grade powder (GUR™ 1020) with a density of 0.93 g/cm^3 was supplied by Ticona GmbH (Werk Ruhrchemie) Germany. The molecular weight of UHMWPE is 2.7×10^6 with particle size ranging between 10 and 300 μm observed using a scanning electron microscope as shown in Fig. 1A and measured using a laser particle size analyzer (Analysette 22; Fritsch GmbH, Germany). The acicular α-Al_2O_3 (~99.9% purity, particle size of 10–30 μm, see Fig. 1B, and density of ~3.953 g/cm^3) was procured from Allied Hi-tech Products, USA. Multiwalled carbon nanotubes (MWCNTs) (95%+ purity, outer diameter of 30–50 nm, inner diameter of 5–15 nm and length up to 10–20 μm with true density of ~2.1 g/cm^3, Fig. 1C) were procured from Nanostructured and Amorphous Materials Inc., NM, USA. In order to prepare the hybrid composites, varying wt.% values of MWCNTs (2, 5 &10%) with fixed wt.% of Al_2O_3 (15%) were added into the UHMWPE matrix, followed by solvent physical blending for 4 h. It was also found that blending did not change the size and shape of the reinforcements MWCNTs and Al_2O_3.

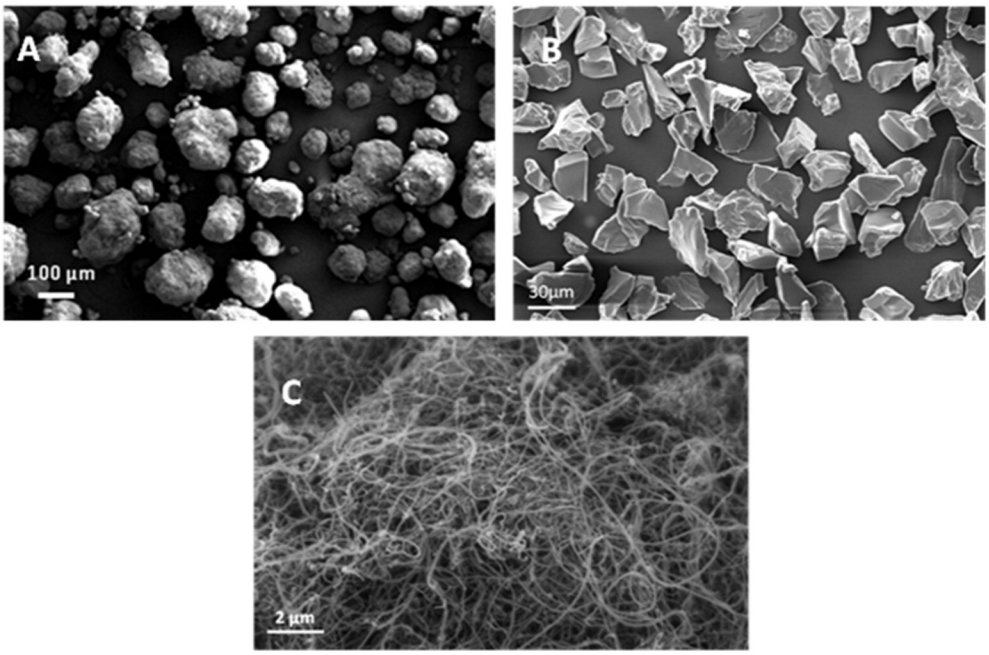

Fig. 1. SEM images of as received (A) UHMWPE, (B) Al_2O_3 and (C) MWCNT powders.

Table 1
Composition, densification and hardness of composites.

Sample ID	Compositions	Densification (% ρ_{th})	Average porosity (%)	Hardness (MPa)
U	UHMWPE	99.8 ± 0.1	0.2 ± 0.1	36.1 ± 3.4
U–15A	UHMWPE–15 wt.% Al_2O_3	96.1 ± 0.0	3.9 ± 0.0	49.5 ± 1.6
U–15A–2C	UHMWPE–15 wt.% Al_2O_3–2 wt.% MWCNT	94.9 ± 0.1	5.1 ± 0.1	54.6 ± 3.4
U–15A–5C	UHMWPE–15 wt.% Al_2O_3–5 wt.% MWCNT	94.0 ± 0.0	6.0 ± 0.1	58.9 ± 3.3
U–15A–10C	UHMWPE–15 wt.% Al_2O_3–10 wt.% MWCNT	93.7 ± 0.1	6.3 ± 0.1	53.3 ± 1.8

Cylindrical pellets ($\Phi = 12$ mm and $t = \sim 3$ mm) were processed by compression molding (SCM-30, M/s Santec Automation Pvt. Ltd., Delhi) at processing temperature of 200 °C and pressure of 7.5 MPa at a hold time of 60 min. The material designation used for the developed composites is shown in Table 1.

2.2. Physical and mechanical characterization

The density of the sintered samples was measured by Archimedes' principle using a CITIZEN CX 220 microbalance with ethanol as an immersion medium (density ~ 0.789 g/cm^3). Bulk hardness of the materials was determined using BAREISS-V-TEST, Bareiss Prüfgerätebau GmbH, Germany, via Vickers macro-indentation experiments. Prior to the indentation test, samples were cloth polished and ultrasonicated for 10–15 min in analytical grade ethanol. Around eight indents were taken at room temperature at 10 g applied load and 10 s dwell time. The indent diagonals were measured to report the hardness values.

2.3. Phase characterization

The X-ray diffraction technique was used to identify the presence of various phases and the degree of crystallinity in compression molded UHMWPE with the reinforcement of Al_2O_3 and MWCNTs. Diffraction patterns were obtained using a Rich-Seifert, 2000D diffractometer operated at 25 kV and 15 mA with Cu-Kα ($\lambda = 1.541$ Å) radiation at a step size of 0.5°/min. Fourier transform infrared (FT-IR, vortex 70, BRUKER) analysis was carried out in the range of 400–4000 cm^{-1}. Further, micro-Raman spectroscopy (WITec GmbH, Germany, Alpha 300) was performed for powder feedstock and compression molded composite pellets to validate the retention of carbon nanotubes by using a green laser with wavelength of 514 nm.

2.4. Surface energy and roughness measurement

The surface energy was calculated using a computer-controlled goniometer system (Dataphysics Contact Angle System OCA) performing sessile drop contact angle measurement with distilled water and n-hexane on the processed Al_2O_3–MWCNT–UHMWPE biopolymeric

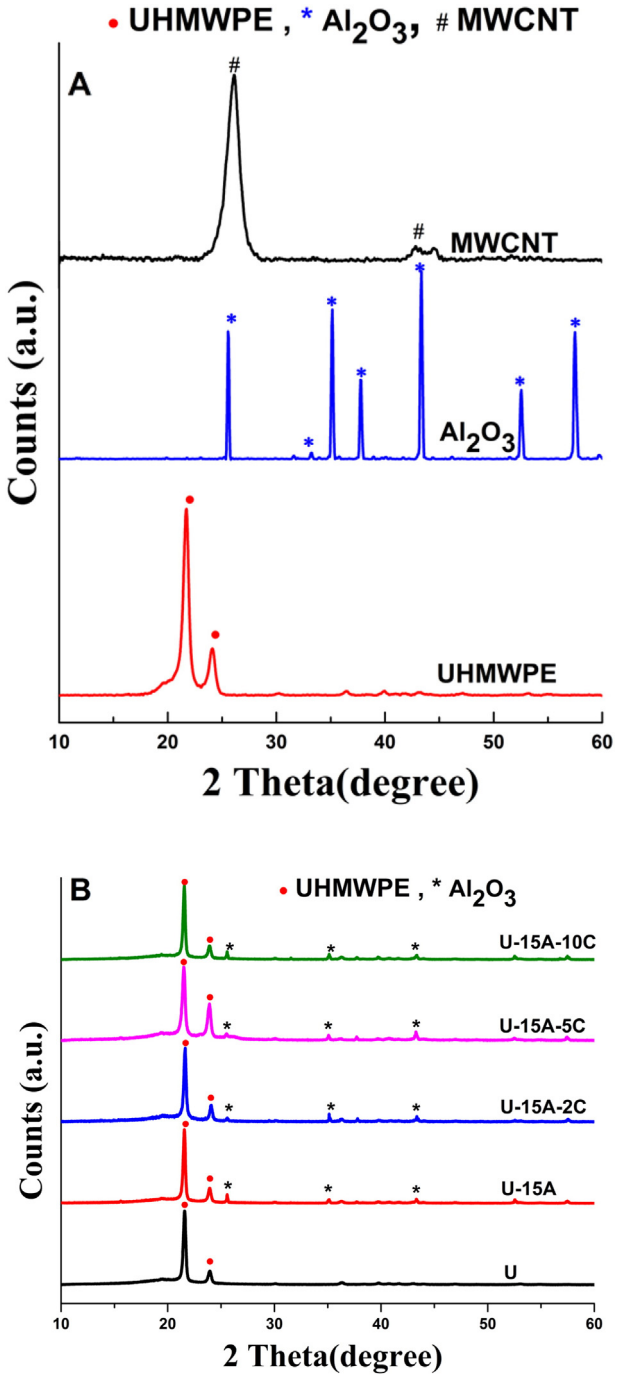

Fig. 3. XRD pattern of (A) starting raw materials and (B) MWCNT and Al_2O_3 reinforced UHMWPE composite pellets respectively.

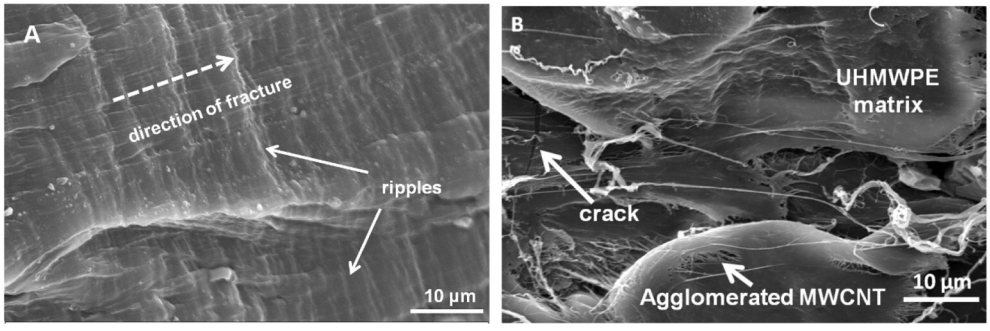

Fig. 2. SEM micrographs of fractured pellets of (A) UHMWPE and (B) U–15A–10C composite.

composites. A water droplet with size of 3–4 mm diameter was gently placed on the sample with the help of a syringe, and a charged coupled device (CCD) camera was used to capture the images. The contact angle on each sample was reported by averaging at least ~10 separate measurements at different locations. The roughness (Ra) of compression molded samples was calculated using an optical profilometer (PS50, Nanovea, Irvine, USA).

2.5. Cellular response

2.5.1. Cell proliferation study

The L929 mouse fibroblast cell line was used for culture on the compression molded Al_2O_3–MWCNT–UHMWPE biopolymer composite pellet, and a gelatin (0.2%) coated glass cover slip was used as a negative control. The samples and control were ultrasonicated to remove any surface oil or impurities, dried at room temperature and further sterilized by 70% ethanol in a UV chamber. L929 cells were cultured in DMEM (Dulbecco's modified Eagles' medium), containing 10% serum and 1% antibiotic with 5% CO_2, 95% humidity and 37 °C temperature. The metabolically active cells with a sub-confluent monolayer of L929 were seeded with cell density of ~5×10^4 on Al_2O_3–MWCNT–UHMWPE biopolymer composite sample surface in 4 well plates. Subsequently, the seeded samples were incubated for 2, 4 and 6 days for proliferation of L929 cells on the material surfaces. After 48 h of incubation period, the adhesion, proliferation and cell counting were reported. Cells were washed twice in PBS (phosphate buffer saline) to completely remove the culture medium and then fixed in 2% glutaraldehyde for 30 min followed by dehydration via a series of 30%, 50%, 70%, 90% and 100% ethyl alcohol solution for 10 min twice with each solution, and then further dehydrated by 100% HMDS (hexamethyldisilazane). The samples were sputter-coated using gold and cell adhesion and proliferation and morphology were observed using a scanning electron microscope (ZEISS, EVO^{R}50).

2.5.2. MTT assay (ISO 10993-5) and calculation of cell density

The MTT assay was performed for varying concentrations of MWCNT (0, 2, 5 and 10 wt.%) and fixed amount of Al_2O_3 (15 wt.%) reinforced UHMWPE compression molded composite pellets with the gelatin coated glass cover slip as a negative control. The viability was done for 2, 4 and 6 days of incubated L929, mouse fibroblast cell line (ATCC). L929 cells were seeded on the samples and control disc in 4 well plates at a density of ~5×10^4 per well. Samples were incubated for 2, 4 and 6 days and then washed with 1× PBS. 50 μl of MTT (5 mg/ml PBS)/100 μl of medium (DMEM) was added in each well and cells were again incubated for 4 h at 37 °C. The precipitation of a tetrazolium component, present in the mitochondria of viable cells, into an insoluble dark-blue formazan was achieved using MTT assay. Then, the formazan crystals were dissolved by adding 200 μl of DMSO (dimethyl sulfoxide) on each sample producing a blue color solution. The solution was then transferred in a 96 well plate and cell viability was measured as an optical density absorbance at 540 nm and 630 nm using an automated microplate reader (Bio-Tek, model ELx800) against DMSO as a blank solvent. The relative optical density was converted to density of living cells/mm^2 using openCV (an open source computer version library software) for the L929-mouse fibroblast cell line under 48 h of incubation period. The statistical analysis of all plotted data was reported by using Student's *t*-test with >95% confidence level ($p < 0.05$).

3. Results and discussion

3.1. Densification and hardness

From Table 1, it is clear that the relative densification of the MWCNT (2, 5 and 10 wt.%) with Al_2O_3 (15 wt.%) reinforced UHMWPE compression molded composite is lower than that of virgin UHMWPE (from 99.7% to 93.7%). It has been observed that a decrease in densification is much more in MWCNTs when compared to that of Al_2O_3, which is attributed to MWCNT entanglement in the viscous polymer matrix during processing. It is also clear from Table 1 that reinforcements such as MWCNTs and Al_2O_3 are enhancing the hardness in comparison to virgin UHMWPE. It was observed that Al_2O_3 (15 wt.%) addition increases the hardness (~37%), in comparison to that of virgin UHMWPE. This amount of extent of Al_2O_3 was chosen after optimization for hardness as well as mechanical properties of composites (kindly see another publication [43]). For the fixed amount of Al_2O_3 content in the UHMWPE matrix, different wt.% values of MWCNTs (2, 5 and 10) were reinforced which gave (10, 19 and 8%) enhancement in the hardness when compared to that of U–15A. The addition of a higher amount (say 10 wt.%) of MWCNTs into the UHMWPE matrix, gave a comparatively lower value of hardness (refer to Table 1), which may be attributed to higher porosity of compression molded composites. The pure UHMWPE has hardness of ~36.1 MPa. The highest hardness has been observed for U–15A–5C of ~58.9 MPa and with the increasing amount of MWCNT reinforcement, the hardness decreases and the porosity increases. During the hardness test no cracks were observed. Fig. 2 represents SEM micrographs of the fractured virgin UHMWPE and U–15A–10C compression molded composite pellets. It is clear from the images that agglomeration and pores were created into the pellets due to higher content of reinforcements. These are the main reasons of low densification for higher content of reinforcements into the UHMWPE matrix composite.

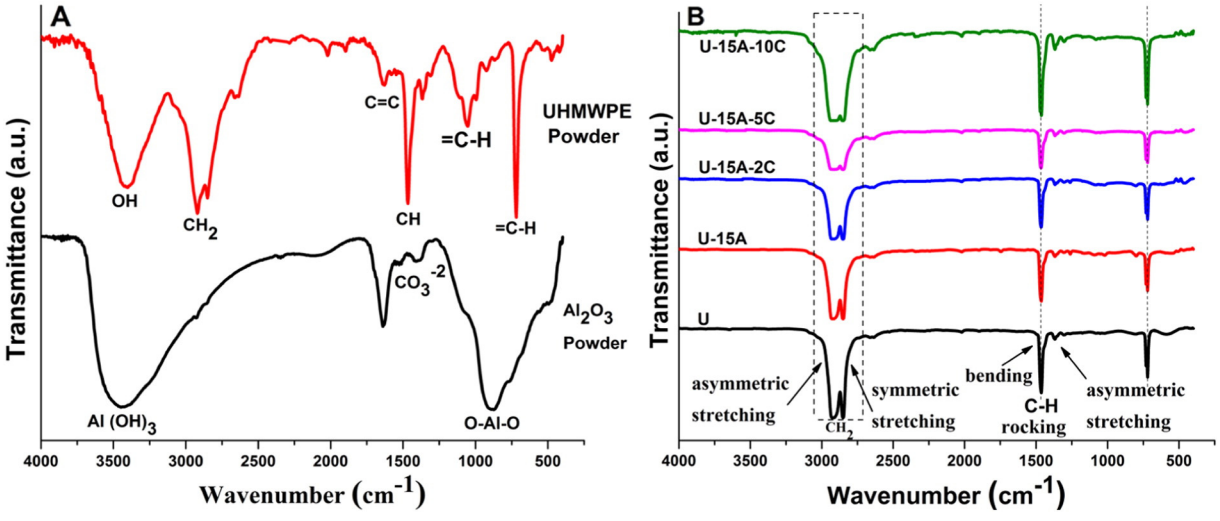

Fig. 4. FT-IR spectra of raw powders: (A) UHMWPE, and Al_2O_3 and (B) MWCNT and Al_2O_3 reinforced UHMWPE composites.

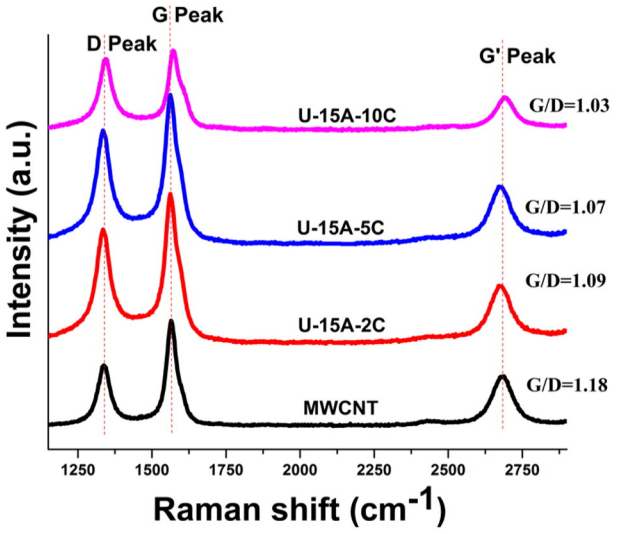

Fig. 5. Raman spectra of pristine MWCNT and MWCNT/Al_2O_3 reinforced UHMWPE composites.

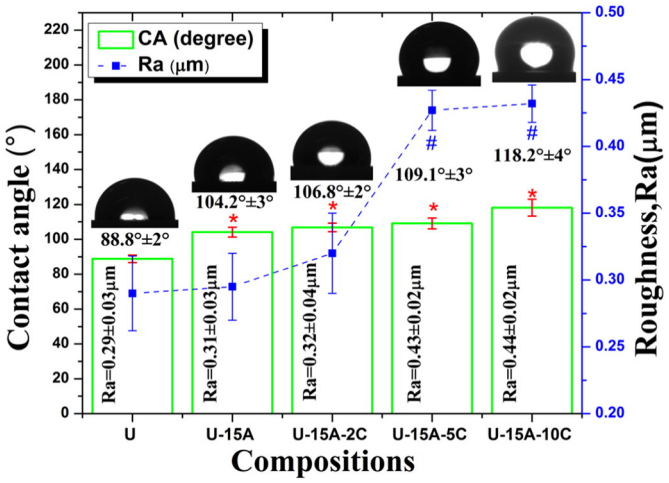

Fig. 6. The influence of reinforcements (Al_2O_3 and MWCNT) on the wettability as well as surface roughness of composites. * means that the contact angle value is significantly different than that on UHMWPE (with $p < 0.002$) and # means that the surface roughness value is significantly different than that of UHMWPE sample (with $p < 0.002$).

3.2. Phase characterization

Fig. 3 shows the XRD patterns of the initial powders (Fig. 3A) and MWCNTs–Al_2O_3 reinforced compression molded UHMWPE polymeric biocomposites (Fig. 3B). The presence of UHMWPE shows two major characteristic peaks at 21.9° and 24.2° while Al_2O_3 peaks well match at 35.2°, 37.9° and 43.6°. MWCNTs show their characteristic peaks at 26.1° and 43.1°. It is observed that the starting peaks of UHMWPE and Al_2O_3 (Fig. 3A) are intact in the processed composites as shown in Fig. 3B. Further, no new phase is detected, which confirms that no reaction phase has formed during processing. X-ray diffraction is complemented with FTIR spectroscopy to allow for the detection of any new (amorphous) phase that might have formed during processing.

Fig. 4 shows the FT-IR spectra of initial UHMWPE, and Al_2O_3 powders (Fig. 4A) and fabricated composites (Fig. 4B). The characteristic bands of UHMWPE at 1464 cm^{-1} C–H bending mode, 1367 cm^{-1} C–H asymmetric bending mode, 730 cm^{-1} and 720 cm^{-1} C–H rocking mode, 2922 cm^{-1} $-CH_2-$ asymmetric stretch and 2850 cm^{-1} $-CH_2-$ symmetric stretch have been observed in FTIR spectra as shown in Fig. 4. A band at 867 cm^{-1} that corresponds to O–Al–O stretching was observed due to the presence of Al_2O_3 in the composition. These findings confirm that no degradation has occurred during processing, and thus, original phases have been retained.

Absence of change in dipole moment in the MWCNTs makes them invisible in the FT-IR spectra. Hence, the micro-Raman technique is used to detect the MWCNTs in the processed composites. Fig. 5 presents the Raman spectrum of initial feedstock MWCNT powder and their composites with fixed amount of the alumina reinforced UHMWPE matrix. The characteristic D (1340 cm^{-1}) and G (1572–1582 cm^{-1}) peaks (similar to that of starting MWCNT) confirm its retention in the compression molded Al_2O_3–MWCNT–UHMWPE biopolymer composites. These G and D peaks correspond to the stretching mode of graphite and defects in the graphite sheet, respectively. The decreased G/D ratio (from 1.18 to 1.03) indicates the damage to MWCNTs during processing.

3.3. Surface energy and roughness measurement

The surface energy was estimated by the sessile drop method and has been reported in Table 2. The contact angle was plotted as a function of roughness with respect to compositions and has been provided in Fig. 6. In order to relate the wetting of processed Al_2O_3–MWCNT–UHMWPE composites with the contributing polar and dispersion fractions, the surface free energy (SFE) and their polar and dispersion parts were calculated by the Owens–Wendt–Rabel–Kaelble geometric mean equations as given below [26].

$$\sigma_s = \sigma_{s1} + \sigma_1 \cdot \cos\theta \tag{1}$$

$$\sigma_1 = \sigma_1^{\,d} + \sigma_1^{\,p} \tag{2}$$

$$\sigma_s = \sigma_s^{\,d} + \sigma_s^{\,p} \tag{3}$$

$$\sigma_{s1} = \sigma_s + \sigma_1 - 2\left(\sqrt{\sigma_s^{\,d} \cdot \sigma_1^{\,d}} + \sqrt{\sigma_s^{\,p} \cdot \sigma_1^{\,p}}\right) \tag{4}$$

$$\frac{1+\cos\theta}{2} \cdot \frac{\sigma_1}{\sqrt{\sigma_1^{\,d}}} = \sqrt{\sigma_s^{\,p}}\sqrt{\frac{\sigma_1^{\,p}}{\sigma_1^{\,d}}} + \sqrt{\sigma_s^{\,d}} \tag{5}$$

where, σ_{s1} is interfacial tension between liquid and solid, σ_s and σ_1 are surface energy of solid surface and surface tension of liquid, respectively, σ_s^d and σ_s^p are dispersion and polar components of solid respectively, and θ is the contact angle between solid and liquid.

Table 2
Surface free energy of composites.

Sample	Total surface energy (mN/m)	Polar component (mN/m)	Dispersion component (mN/m)	Polar fraction	Dispersion fraction
U	23.20	5.16	18.04	0.223	0.777
U–15A	21.55	3.61	17.93	0.168	0.832
U–15A–2C	19.01	1.12	17.89	0.059	0.941
U–15A–5C	18.58	0.56	18.38	0.030	0.970
U–15A–10C	17.75	0.05	17.70	0.003	0.997

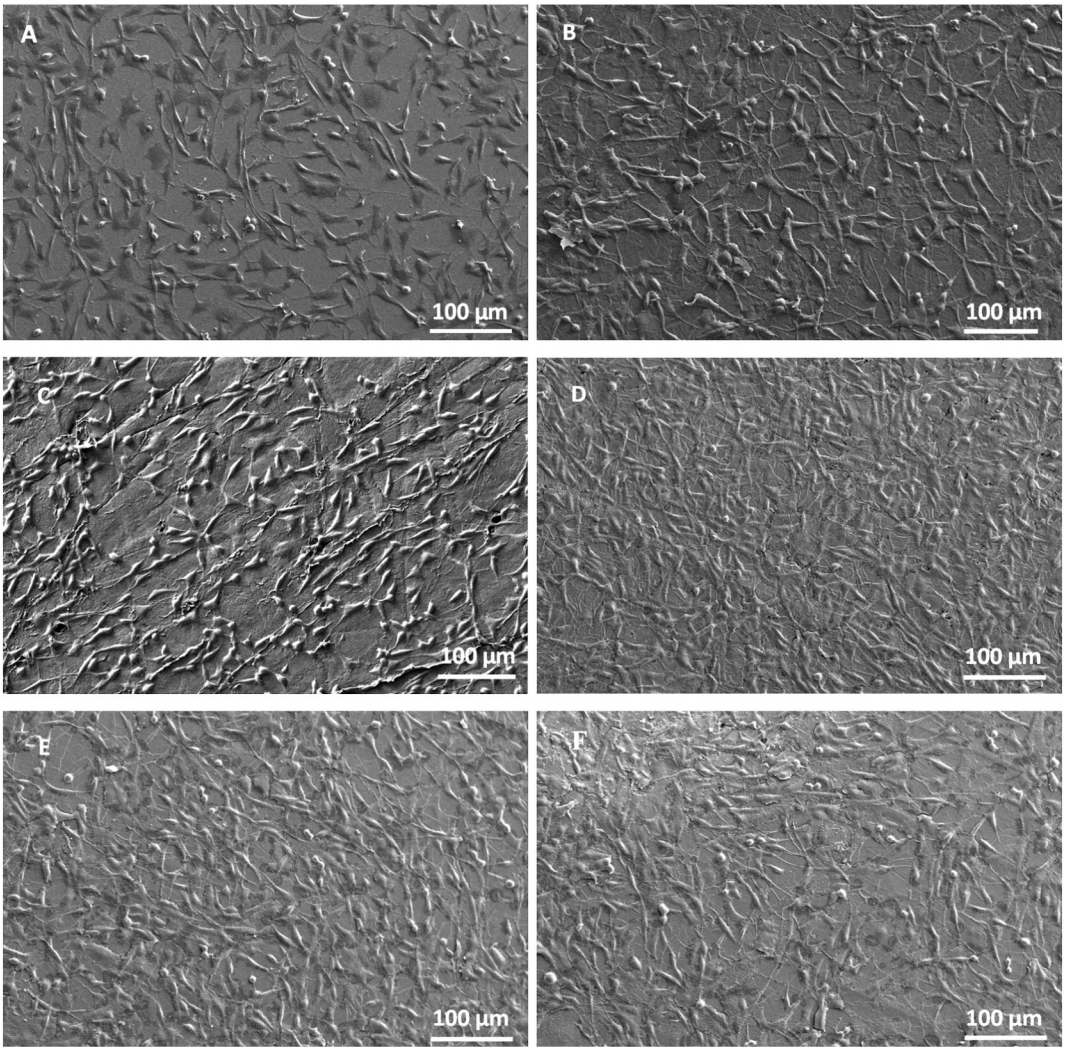

Fig. 7. Scanning electron micrographs of L929 mouse fibroblast cells grown on (A) control gelatin coated cover slip disc and (B) U, (C) U–15A, (D) U–15A–2C, (E) U–15A–5C and (F) U–15A–10C composites (in 48 h incubation period).

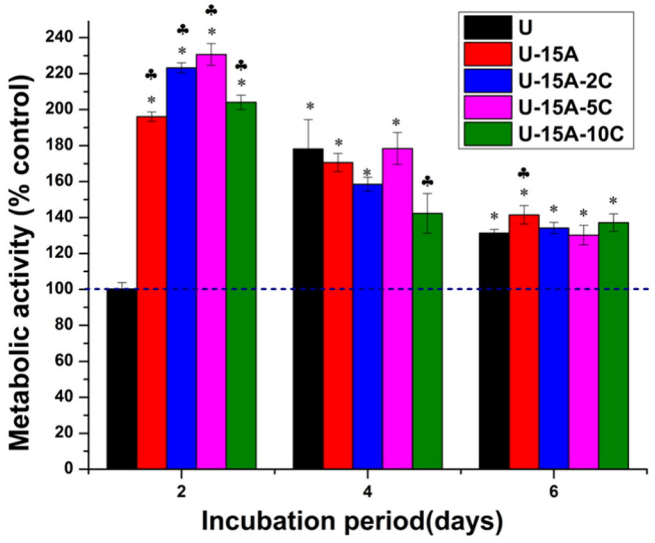

Fig. 8. MTT assay results showing the relative number of metabolically active L929 cells on UHMWPE based composites (* means that the cell count is significantly different than that on a control sample, with $p < 0.002$ and ♣ means that the cell count is significantly different than that on neat UHMWPE sample, with $p < 0.002$).

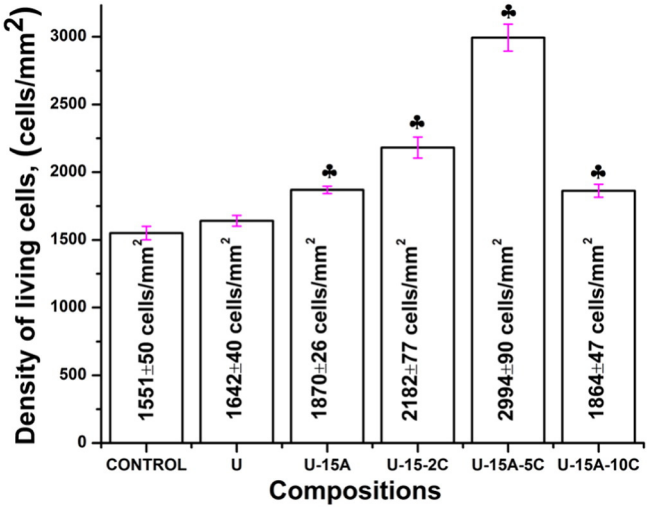

Fig. 9. Plot represents the density of metabolically active L929 mouse fibroblast cells during 48 h culture period. The numbers of living cells were counted from the selected areas (from SEM images of corresponding compositions, Fig. 7). (♣ means that the cell density count is significantly different than that on a control sample (gelatin coated cover slip, with $p < 0.002$).

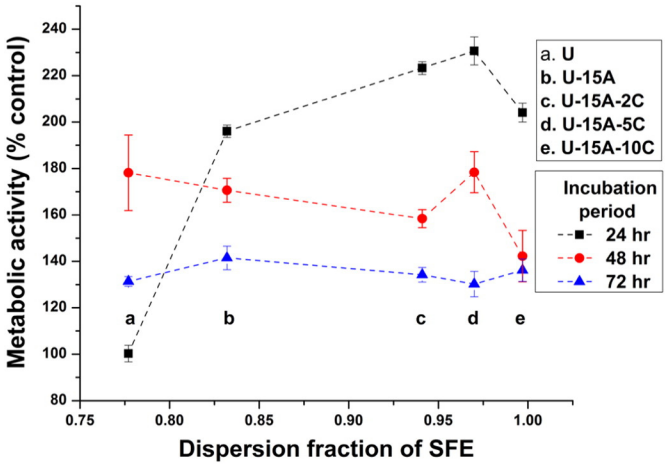

Fig. 10. Correlation between cell densities with dispersion fractions of surface free energy (SFE) for 1-, 2- and 3-day incubation period.

Fig. 6 reveals that the contact angle increases with increasing amount of reinforcement of Al_2O_3 and MWCNTs, when compared to that of virgin UHMWPE (~88°). The U–15A–10C composite reinforced with MWCNTs (10 wt.%) and Al_2O_3 (15 wt.%) has shown a higher value of contact angle (~118°, see Fig. 6), which is attributed to decreased surface energy (17.75 mN/m) and high dispersion fraction (0.997) when compared with U–15A (only 15 wt.% Al_2O_3 reinforced) that shows a contact angle of 104.2° with surface energy of 21.55 mN/m (dispersion fraction of 0.832). This result indicates that the surface energy and its dispersion fraction play a significant role for the cellular growth on UHMWPE–Al_2O_3–MWCNT composites. A synergistic ~33% increase in the contact angle shows higher hydrophobicity due to its higher dispersion fraction of free energy. Further, the contact angle is effectively affected by wt.% of reinforcements since the surface roughness is in the same order of magnitude (Fig. 6).

3.4. Cellular response

3.4.1. Qualitative: cell proliferation study

The SEM images of 48 h cultured L929 mouse fibroblast cells are depicted in Fig. 7A–F, which confirms its unhindered proliferation on the processed composites. It may be concluded that the materials possess good cytocompatibility towards the L929 mouse fibroblast cell line and spread without any toxicity on each Al_2O_3–MWCNT–UHMWPE biopolymeric composite surface.

3.4.2. Quantitative: MTT assay (ISO 10993-5) and calculation of cell density

The MTT assay results on the compression molded composites with varying amounts of MWCNT (2, 5, and 10 wt.%) with fixed amount of Al_2O_3 (15 wt.%) reinforced UHMWPE are shown for 2-, 4- and 6-day

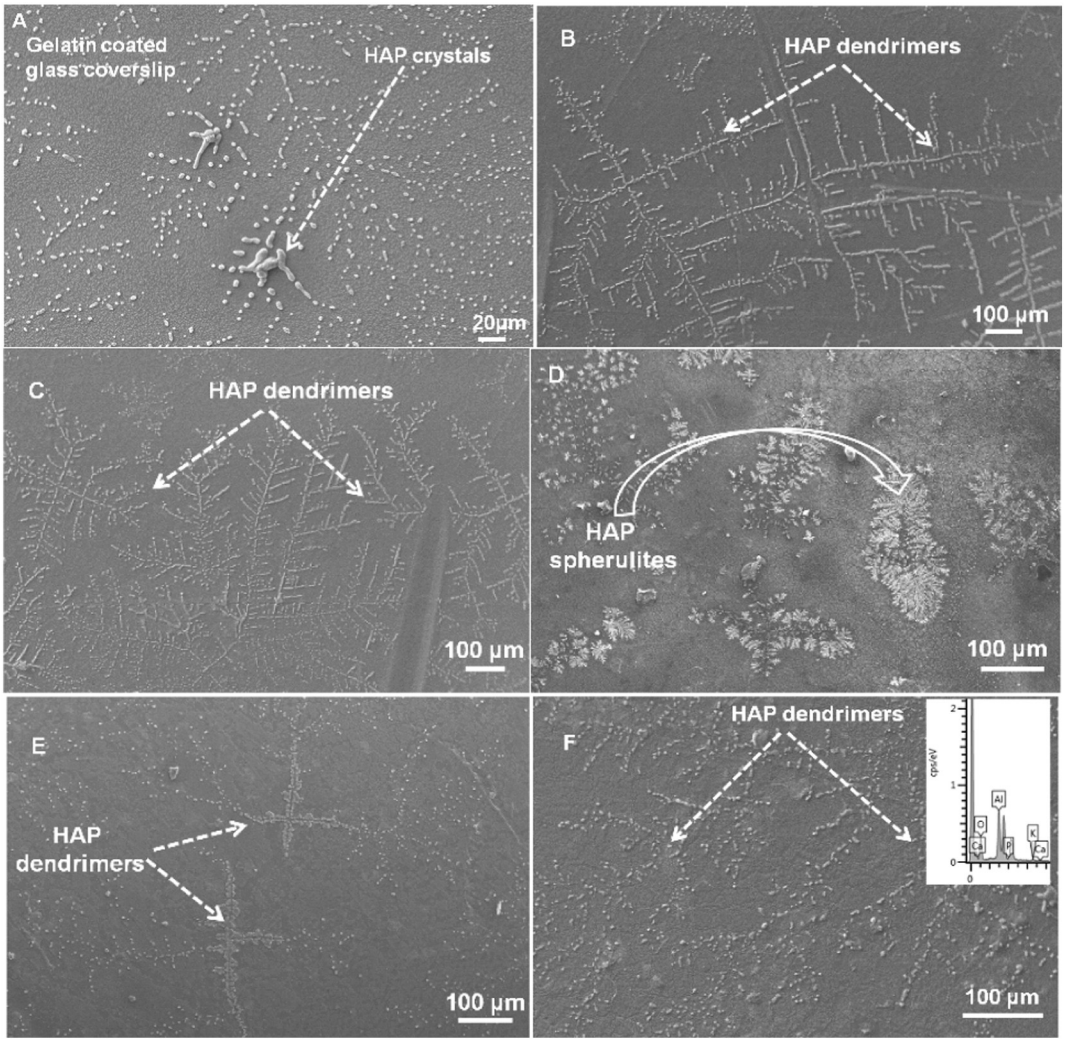

Fig. 11. Scanning electron micrographs of apatite formation on the material surfaces in the presence of DMEM culture media of (A) negative control and (B) U, (C) U–15A, (D) U–15A–2C, (E) U–15A–5C and (F) U–15A–10C composites (during 48 h incubation period).

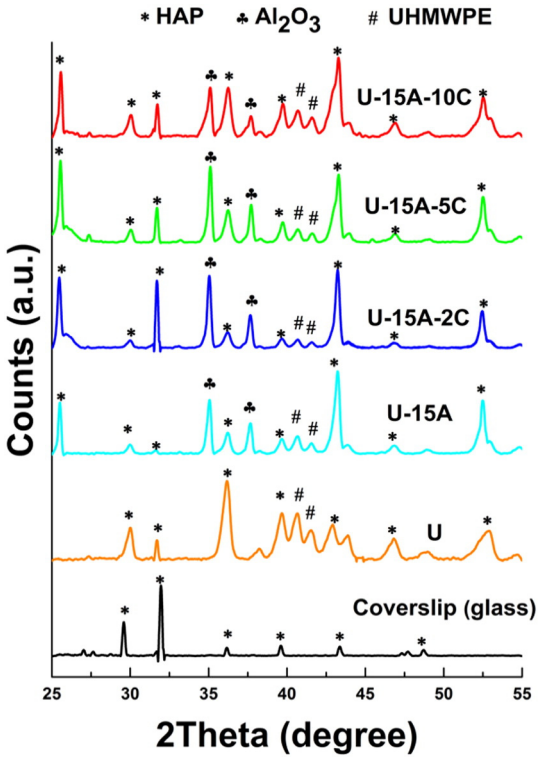

Fig. 12. XRD pattern of apatite minerals (HAP) grown on the surface of negative control (cover slip), UHMWPE as well as MWCNT and Al_2O_3 reinforced UHMWPE composite pellets.

culture in Fig. 8, where the gelatin coated glass cover slip was taken as a negative control. The metabolic activity of the negative control was taken as 100%. It was observed that with time, the metabolically active cell density decreases for 48 h or more incubation periods (except virgin UHMWPE) although a same trend was observed for all other compositions, which may be attributed to earlier confluence of cells, unavailability of free space at the surface for further proliferation, and enhancement of polar fraction of SFE due to apatite mineralization. It may be noted that after 48 h of incubation period, a sudden increase in the cell density of UHMWPE is attributed to the availability of space at the surface for cell proliferation in comparison to other samples. It is predicted that up to 72 h of incubation periods, the cells become confluent at the surfaces and suppress the cell density at all compositions. From Fig. 8, it may be concluded that the composites retain their cytocompatibility and quantification of which is presented as the L929-mouse fibroblast cell count per unit area (numbers/mm^2) at 48 h of incubation in Fig. 9. A trend similar to that observed in Fig. 8 can be compared, where the highest cell density was observed for U–15A–5C composites.

On a first-hand look, it appears that a higher dispersion component (see Table 2) and contact angle (Fig. 6) do not gel well in terms of dictating the metabolic activity (see Figs. 8 and 9), which is insinuated from a higher dispersion fraction of U–15A–10C eliciting a lower cell density when compared to that of U–15A–5C. Further, a reduction in the metabolic activity (with respect to control sample) can be observed in Fig. 10. So, something is definitely occurring during the incubation that is changing the surface properties, and thus, the cellular growth. It is anticipated that the formation of apatite (during incubation) changes the polar fraction of SFE, and thus affects cell-proliferation and growth. Thus, the next step involves verification of apatite formation in a 48 h cultured sample using SEM and EDS, and the fraction of apatite content is quantified using X-ray diffraction.

From Fig. 10, it is clear that the growth of metabolically active cells is directly related to the dispersion fraction of SFE up to 24 h of incubation period, while the metabolic activity became independent at higher incubation periods (48 and 72 h). Since lower cell density was observed for 48 h and 72 h of incubation period of cell culture, when compared to that at 24 h culture, it is indicated that some changes are occurring on sample surface to result such a cell growth in comparison to that of the negative control. In order to check the surface compositional change at 48 h of incubation period, samples were immersed in media under same environmental conditions and phase and elemental analyses were characterized using X-ray diffraction pattern and scanning electron microscopy (with energy dispersive spectroscopy), respectively.

3.4.3. Quantification of apatite mineralization

The mineralization of hydroxyapatite (HAP) on the material's surface at 48 h incubation period is shown in Fig. 11A–F, where the formation of apatite crystals is evident (and elemental analysis reveals presence of Ca and P in the inset of Fig. 11F) and confirmed via X-ray diffraction in Fig. 12. The SEM micrographs (Fig. 11) show dendrimers of HAP mineralized crystals that nucleate on the composite surfaces. The morphology of mineralized HAP crystals is a complex phenomenon which depends on the mineral contents (Ca/P ratio), pH of the medium, interaction with the immersion solutions, absorption as well release of ions at the interface, and nucleation and growth kinetics [44–48]. The content of deposited HAP is quantified by taking the integrated area of HAP peaks (divided by all other peaks) for comparison (see Table 3). HAP precipitation is observed to increase with increasing amounts of Al_2O_3 and MWCNTs in the UHMWPE matrix. But, the U–15A–5C composite elicited a comparatively lower amount of HAP formation than others (Fig. 11E), and its corresponding dispersion fraction is related to precipitated apatite in Fig. 13. It can be recollected (from Figs. 8–10) that U–15A–5C has shown the highest count of metabolically active cells, which very well correlates with the fact that dispersion fraction has assisted the rapid growth of cells. Intuitively, the presence of HAP should correlate with cell-growth, but it must be noted that the extent of the MWCNT content on the surface is dictated by their dispersion, and so the precipitation of apatite is affected by the same. High HAP mineralization in SBF also indicates that high chances of cell-confluence exist, and thus, further cell-growth is restricted. Thus, the higher the apatite formation, the higher is the polar fraction that lowers the dispersion fraction of surface energy (see Fig. 13), and results in reduced cell activity due to its confluence (as observed at 48 h of incubation period).

It is well known that the adsorbed cell density depends on the material surface properties such as surface free energy, roughness, porosity and presence of reactive functional moieties like –OH, –NH_2, –COOR, –C–O and C═O [49,50]. As described in Fig. 10, the cell density

Table 3
Fractional phase extent of mineralized apatite on the material surfaces and corresponding wettability and surface free energy (SFE) after 48 h incubation in SBF.

Sample-ID	Contact angle with H_2O (°)	Contact angle with n-hexane (°)	Total surface free energy (SFE) (mN/m)	HAP fraction [HAP / (HAP + UHMWPE + Al_2O_3)] (%)	Dispersion fraction of surface free energy (SFE)
U	66.0 ± 3.6	13.5 ± 1.0	40.26 ± 3.1	48.5 ± 3.3	0.43
U–15A	54.1 ± 2.1	13.5 ± 0.5	45.39 ± 1.6	51.8 ± 3.5	0.39
U–15A–2C	55.5 ± 2.5	12.2 ± 2.2	49.76 ± 4.2	55.4 ± 3.6	0.37
U–15A–5C	60.4 ± 3.4	13.6 ± 1.5	41.28 ± 3.1	49.5 ± 3.1	0.45
U–15A–10C	48.6 ± 1.0	11.8 ± 1.2	50.53 ± 6.1	60.1 ± 3.9	0.35

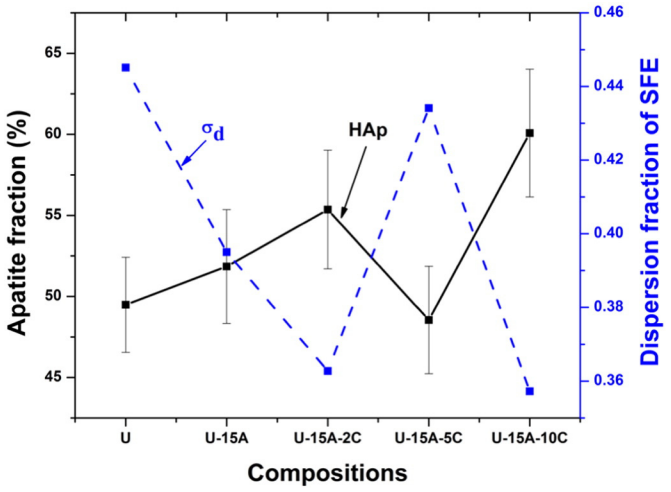

Fig. 13. Graph showing the correlation of dispersion fraction with percent fraction of mineralized apatite at the material surfaces after 48 h of incubation period.

proportionally correlated with the dispersion fraction of surface free energy up to 24 h of incubation period, but, as observed, the reinforcements of Al_2O_3 and MWCNTs tend to enhance the dispersion fraction of SFE (Fig. 10) leading to enhanced protein adsorption at the surface. Gupta et al. [50] has reported that the dispersion fraction plays a much more significant role in protein adsorption rather than the total free energy or surface roughness. Concurrently, the decrease in dispersion fraction with increasing HAP precipitation is observed in Fig. 13. Thereafter, the precipitation of apatite lowers the dispersion fraction and limits the cellular activity, which might result due to earlier and rapid cell-growth, followed by confluence of cells. This hypothesis is confirmed by the direct correlation of apatite mineralization (Fig. 13) with 48 h of metabolic activity (Fig. 10).

The virgin UHMWPE shows a lower value of contact angle (88.8 ± 2°) and dispersion fraction (0.777) with a higher value of SFE (23.20 mN/m) in comparison to other compositions, as reported in Fig. 6 and Table 2. The lower dispersion fraction, leads to lower density of viable cells (Figs. 9 and 10), but, the addition of Al_2O_3 enhances the contact angle (88.8 ± 2° to 104.2 ± 3°), dispersion fraction (0.777 to 0.832), and cell viability (1642 ± 40 to 1870 ± 26 cells/mm^2) with a decrease in the SFE on the 2nd day of incubation period. While decreased cell viability was observed for 48 h in U–15A, the mineralized amount of apatite has enhanced (48.5 ± 3.3% to 51.8 ± 3%) and the dispersion fraction of SFE has reduced (from 0.43 to 0.39) when compared to that of virgin UHMWPE. Contrastingly, the reinforcement of MWCNTs enhances hydrophobicity (88.8 ± 2° to 118.2 ± 4°) compared to virgin UHMWPE as well as Al_2O_3 reinforced composites and decreases the SFE (23.20 mN/m to 17.75 mN/m) with an increase in the dispersion fraction (from 0.777 to 0.997) as well as cell viability from 1642 ± 40 to 2994 ± 2690 cells/mm^2 (Figs. 6 & 9) for 24 h of incubation period. A summary of these observations for 24 h of incubation period of cell culture is schematically presented in Fig. 14 that shows an increase in cell-density with increasing amount of Al_2O_3 and MWCNTs in the UHMWPE matrix.

Contrastingly, for 48 h incubation period of cell culture, a significant amount of apatite mineralization was observed (varying from 48.5 ± 3.3% to 60.1 ± 3.9%) in comparison to that of UHMWPE and alumina based compositions, which lowers the dispersion fraction of SFE from 0.43 to 0.35 and reduced the cell viability (Table 3). Thus, a decrease in the metabolic activity can be attributed to the significant precipitation of apatite on the surfaces (see Table 3), which subsequently lowers the dispersion fraction of SFE. From the above observations it is clear that the Al_2O_3 and MWCNT reinforcement increases the hydrophobicity and dispersion fraction of SFE, which enhances the proliferation of L929 mouse fibroblast cells in comparison to virgin UHMWPE.

Since metabolic activity strongly depends on the dispersion fraction of SFE (instead of total SFE), the dispersion fraction can be enhanced by reinforcement of more hydrophobic moieties like CNTs and by engineering the surface hydrophobicity via functionalization to add long saturated hydrocarbon chains. Thus, the enhanced metabolic activity of a material can be utilized for affixing an acetabular cup liner on the pelvis side, but engineered lower dispersion fraction on the opposite side can render reduced cell adhesion (and good articulation) at the ball-joint mating surface.

4. Conclusions

Polymeric biocomposites reinforced with MWCNTs and Al_2O_3 were successfully processed by using the compression molding method. The total surface free energy (TSFE) was strongly affected (~23%) by MWCNT reinforcement in UHMWPE when compared to that of Al_2O_3 reinforcement (~7%). Consequently, the polar and dispersion fractions of SFE were also altered by reinforcements. MWCNT with Al_2O_3 reinforced UHMWPE composites showed higher hydrophobicity (~118.2° ± 4°) in comparison to only Al_2O_3 reinforcement (104.2° ± 3°) and virgin UHMWPE (88.8° ± 2°). Up to 24 h of incubation period, the cellular

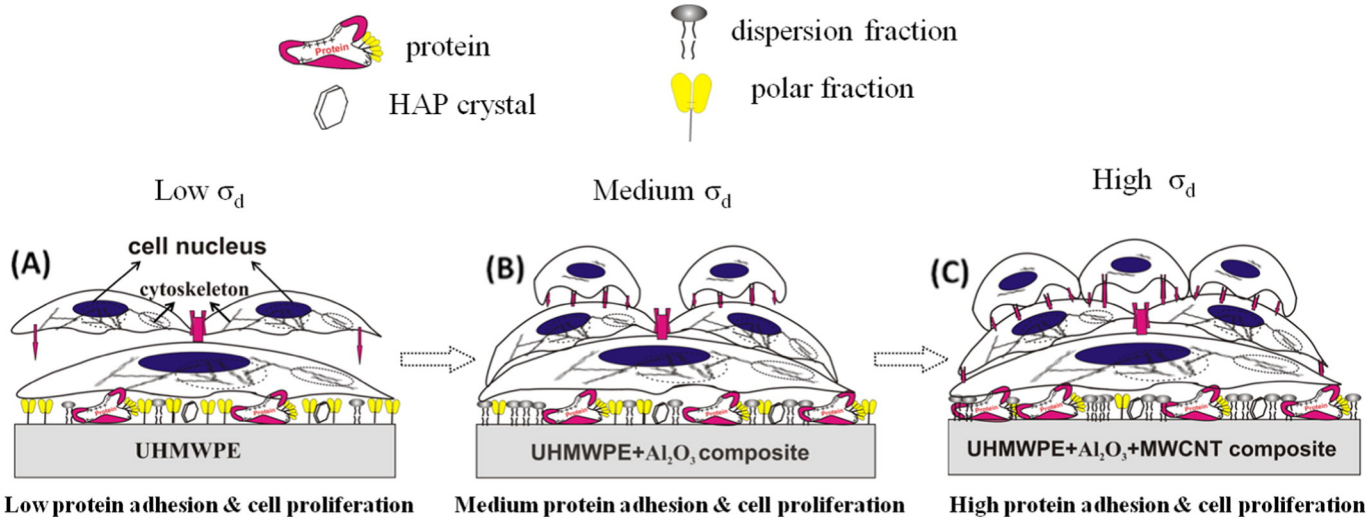

Fig. 14. Schematic illustration of the mechanism of cell-adhesion and proliferation with the effect of Al_2O_3 and MWCNT reinforcement on UHMWPE based composites. Here (A), (B) and (C) represent the cell adhesion at the virgin UHMWPE, alumina reinforced composite, and UHMWPE–Al_2O_3–MWCNT composite respectively and σ_d represents the dispersion fraction of SFE.

response of the composites was mainly governed by the initial surface free energy, and cell viability was observed to be directly dependent on the dispersion fraction of SFE. The original SFE of the composites has been changed significantly (enhanced by ~72% for UHMWPE and ~184% for the U–15A–10C composite, respectively) for higher incubation periods (48 h or more) due to apatite formation (60.1 ± 3.9% by fraction) on the material surfaces, which decreases the dispersion fraction of surface free energy and results in cell-confluences to reduce the metabolic activity. It may be concluded that the cell growth is predominantly governed by the dispersion fraction of SFE. Thus, the optimized MWCNT–Al_2O_3 reinforced UHMWPE biocomposites may be accordingly engineered to provide the most suitable composite material for articulating surface bioimplant applications.

Acknowledgments

The authors acknowledge the funding from the Department of Biotechnology (grant number: BT/PR11224/MED/32/57/2008), Government of India and also thank Celanese Pte. Ltd., Keppel Towers, Singapore, for providing UHMWPE medical grade (GUR 1020) on gratis.

References

[1] J. Black, Biological Performance of Materials: Fundamentals of Biocompatibility, 2nd ed. Marcel Dekker, New York, 1992. 400.
[2] S. Ramakrishna, et al., Biomedical applications of polymer-composite materials: a review, Compos. Sci. Technol. 61 (9) (2001) 1189–1224.
[3] Y. Cohen, D.M. Rein, L. Vaykhansky, A novel composite based on ultra-high molecular weight polyethylene, Compos. Sci. Technol. 57 (1997) 1149–1154.
[4] M.K. Musib, A review of the history and role of UHMWPE as a component in total joint replacements, Int. J. Biol. Eng. 1 (1) (2011) 6–10.
[5] C.Y. Tang, et al., Enhanced wear performance of ultrahigh molecular weight polyethylene cross linked by organosilane, J. Mater. Sci. Mater. Med. 13 (2002) 1065–1069.
[6] S. Perni, M.G. Kong, P. Prokopovich, Cold atmospheric pressure gas plasma enhances the wear performance of ultra-high molecular weight polyethylene, Acta Biomater. 8 (3) (2012) 1357–1365.
[7] J.L. Tipper, et al., Isolation and characterization of UHMWPE wear particles down to ten nanometers in size from in vitro hip and knee joint simulators, J. Biomed. Mater. Res. A 78A (3) (2006) 474–480.
[8] N. Inoue, et al., Composite materials in bio-medical engineering, Mater. Tech. 92 (1994) 23–26.
[9] C. Silverton, et al., The prosthesis–bone interface adjacent to tibial components inserted without cement, J. Bone Joint Surg. 78 (A(3)) (1996) 340–347.
[10] S.L. Ruan, et al., Toughening high performance ultrahigh molecular weight polyethylene using multiwalled carbon nanotubes, Polymer 44 (19) (2003) 5643–5654.
[11] L. Jin, C. Bower, O. Zhou, Alignment of carbon nanotubes in a polymer matrix by mechanical stretching, Appl. Phys. Lett. 73 (1998) 1197.
[12] C. Bower, et al., Deformation of carbon nanotubes in nanotube–polymer composites, Appl. Phys. Lett. 74 (22) (1999) 3317.
[13] K. Balani, A. Agarwal, Process map for plasma sprayed aluminum oxide–carbon nanotube nanocomposite coatings, Surf. Coat. Technol. 202 (2008) 4270–4277.
[14] J.E. Tercero, et al., Effect of carbon nanotube and aluminum oxide addition on plasma-sprayed hydroxyapatite coating's mechanical properties and biocompatibility, Mater. Sci. Eng. C 29 (2009) 2195–2202.
[15] K. Balani, et al., Plasma-sprayed carbon nanotube reinforced hydroxyapatite coatings and their interaction with human osteoblasts in vitro, Biomaterials 28 (2007) 618–624.
[16] M.A.F. Afzal, et al., Functionally graded hydroxyapatite–alumina–zirconia biocomposite: synergy of toughness and biocompatibility, Mater. Sci. Eng. C 32 (2012) 1164–1173.
[17] E.C. Preedyetal, Adhesive forces and surface properties of cold gas plasma treated UHMWPE, Colloids Surf. A Physicochem. Eng. Asp. 460 (2014) 83–89.
[18] X. Wu, C. Wu, G. Wang, A crosslinking method of UHMWPE irradiated by electron beam using TMPTMA as radiosensitizer, J. Appl. Polym. Sci. 127 (1) (2013) 111–119.
[19] J. Zhou, F. Yan, Improvement of the tribological behavior of ultra-high-molecular-weight polyethylene by incorporation of poly(phenyl p-hydroxyzoate), J. Appl. Polym. Sci. 96 (6) (2005) 2336–2343.
[20] Y. Chen, et al., Structure and tensile properties change of LDPE/UHMWPE blends via solid state shear milling, J. Appl. Polym. Sci. 130 (4) (2013) 2487–2493.
[21] H. Pang, Y. Bao, Preparation and properties of carbon nanotube/binary-polymer composites with a double-segregated structure, J. Appl. Polym. Sci. 131 (2) (2014).
[22] Y. An, et al., Friction and wear properties of graphene oxide/ultrahigh-molecular-weight polyethylene composites under the lubrication of deionized water and normal saline solution, J. Appl. Polym. Sci. 131 (1) (2013).
[23] M.C. Galetz, T. Blab, H. Ruckdäschel, Carbon nanofibre-reinforced ultrahigh molecular weight polyethylene for tribological applications, J. Appl. Polym. Sci. 104 (6) (2007).
[24] A. Huang, R. Su, Y. Liu, Effects of a coupling agent on the mechanical and thermal properties of ultrahigh molecular weight polyethylene/nano silicon carbide composites, J. Appl. Polym. Sci. 129 (3) (2012) 118–122.
[25] J. Zhou, F. Yan, Effect of polyethylene-graft-maleic anhydride as a compatibilizer on the mechanical and tribological behaviors of ultrahigh-molecular-weight polyethylene/copper composites, J. Appl. Polym. Sci. 93 (2) (2004) 948–955.
[26] A. Gupta, et al., Compression molded ultra high molecular weight polyethylene–hydroxyapatite–aluminum oxide–carbon nanotube hybrid composites for hard tissue replacement, J. Mater. Sci. Technol. 29 (6) (2013) 514–522.
[27] S.R. Bakshi, J.E. Tercero, A. Agarwal, Synthesis and characterization of multiwalled carbon nanotube reinforced ultra high molecular weight polyethylene composite by electrostatic spraying technique, Compos. Part A 38 (2007) 2493–2499.
[28] S.R. Bakshi, et al., Nano-mechanical and nano-scratch characterization of UHMWPE and UHMWPE–5 wt.% MWNT coatings on a steel substrate, J. Miner. Met. Mater. (JOM) (2007) 50–53.
[29] J.H. Lee, et al., Wear properties of 3-aminopropyltriethoxysilanefunctionalized carbon nanotubes reinforced ultra high molecular weight polyethylene nanocomposites, Polym. Eng. Sci. 50 (2010) 1433–1439.
[30] E. Inghama, J. Fisherb, The role of macrophages in osteolysis of total joint replacement, Biomaterials 26 (2005) 1271–1286.
[31] Y. Liu, S.K. Sinha, Wear performances of UHMWPE composites with nacre and CNTs, and PFPE coatings for bio-medical applications, Wear 300 (2013) 44–54.
[32] L. Li, et al., Carbon nanotube induced polymer crystallization: the formation of nanohybrid shish–kebabs, Polymer 50 (22) (2009) 953–965.
[33] R. Haggenmueller, J.E. Fischer, K.I. Winey, Single wall carbon nanotube/polyethylene nanocomposites: nucleating and templating polyethylene crystallites, Macromolecules 39 (2006) 2964–2971.
[34] G. Sui, et al., Structure, mechanical properties and friction behavior of UHMWPE/HDPE/carbon nanofibers, Mater. Chem. Phys. 115 (2009) 404–412.
[35] B.X. Yang, et al., Mechanical reinforcement of polyethylene using polyethylene-grafted multiwalled carbon nanotubes, Adv. Funct. Mater. 17 (2007) 2062–2069.
[36] Y.S. Zoo, et al., Effect of carbon nanotube addition on tribological behavior of UHMWPE, Tribol. Lett. 16 (2004) 305–309.
[37] K. Herkendell, et al., Domination of volumetric toughening by silver nanoparticles over interfacial strengthening of carbon nanotubes in bactericidal hydroxyapatite biocomposite, Mater. Sci. Eng. C 34 (2014) 455–467.
[38] M.A.F. Afzal, et al., Bactericidal effect of silver-reinforced carbon nanotubes and hydroxyapatite composites, J. Biomater. Applica. 27 (2013) 967–968.
[39] M. Szubert, K. Adamska, M. Szybowicz, The increase of apatite layer formation by the poly(3-hydroxybutyrate) surface modification of hydroxyapatite and β-tricalcium phosphate, Mater. Sci. Eng. C 34 (2014) 236–244.
[40] C.F. Koch, et al., Pulsed laser deposition of hydroxyapatite thin films, Mater. Sci. Eng. C 27 (2007) 484–494.
[41] A.A. Zadpoor, Relationship between in vitro apatite-forming ability measured using simulated body fluid and in vivo bioactivity of biomaterials, Mater. Sci. Eng. C 35 (2014) 134–143.
[42] M. Szubert, et al., The increase of apatite layer formation by the poly(3-hydroxybutyrate) surface modification of hydroxyapatite and β-tricalcium phosphate, Mater. Sci. Eng. C 34 (2014) 236–244.
[43] A.K. Patel, P. Trivedi, K. Balani, Processing and mechanical characterization of compression-molded ultrahigh molecular weight polyethylene biocomposite reinforced with aluminum oxide, J. Nanosci. Nanoeng. Appl. 4 (3) (2014) 1–11.
[44] C. Drouet, Apatite formation: why it may not work as planned, and how to conclusively identify apatite compounds, BioMed Res. Int. 13 (2013) 1–12.
[45] H. Anahi, et al., Biomimetic apatite formation on Ultra-High Molecular Weight Polyethylene (UHMWPE) using modified biomimetic solution, J. Mater. Sci. Mater. Med. 20 (2009) 1215–1222.
[46] R.J. Dekker, et al., Bone tissue engineering on amorphous carbonated apatite and crystalline octacalcium phosphate-coated titanium discs, Biomaterials 26 (25) (2005) 5231–5239.
[47] S. Graham, P.W. Brown, Reactions of octacalcium phosphate to form hydroxyapatite, J. Cryst. Growth 165 (1–2) (1996) 106–115.
[48] F. Barrere, et al., Biomimetic calcium phosphate coatings on Ti6Al4V: a crystal growth study of octacalcium phosphate and inhibition by Mg^{2+} and HCO_3^-, Bone 25 (2, Supplement 1) (1999) 107S–111S.
[49] Y. Arima, H. Iwata, Effects of surface functional groups on protein adsorption and subsequent cell adhesion using self-assembled monolayers, J. Mater. Chem. 17 (2007) 4079–4087.
[50] A. Gupta, et al., Dependence of protein adsorption on wetting behavior of UHMWPE–HA–Al_2O_3–CNT hybrid biocomposites, JOM 64 (4) (2012).